TE-Polarized Bessel-Beam Launchers for Wireless Power Transfer at Millimeter Waves: Theory, Design, and Experimental Validation

TE-Polarized Bessel-Beam Launchers for Wireless Power Transfer at Millimeter Waves: Theory, Design, and Experimental Validation

Francesca Benassi, *Member, IEEE,* Edoardo Negri, *Graduate Student Member, IEEE,* Walter Fuscaldo, *Senior Member, IEEE,* Giacomo Paolini, *Member, IEEE,* Francesco Maita, Paolo Burghignoli, *Senior Member, IEEE,* Diego Masotti, *Senior Member, IEEE,* Alessandro Galli, *Member, IEEE,* and Alessandra Costanzo, *Fellow, IEEE*

***Abstract*—Transverse-electric (TE) polarized Bessel-beam launchers working at millimeter-wave frequencies are theoretically described, simulated, realized, and experimentally validated. A limited-diffractive near-field distribution up to the so-called *nondiffractive-range* distance of about 30 mm has been obtained in this work. To generate a *pure* TE leaky mode, avoiding undesired transverse-magnetic (TM) field components, an innovative feeding scheme is designed consisting of a circular array of four radial slots. In order to enhance compactness, the four slots are excited through a single-port meandered microstrip feeding network, which has been optimized to ensure the same signal distribution exciting the slots while minimizing unwanted coupling among them. Full-wave simulations allowed for accurately designing a resonant cavity at 30 GHz able to generate a TE-polarized Bessel beam. Two launchers of this kind are then exploited to create a *wireless power transfer* (WPT) link whose performance is firstly computed numerically and then verified by means of measurements for different transmitter-receiver distances, namely 25, 35, and 48 mm. These values respectively fall within, in proximity of, and away from the nondiffractive region of the transmitting device, showing an increasing WPT performance deterioration, as expected. For the case of a 25-mm distance, the evaluated $|S_{21}|$ is -12 dB, in excellent agreement between full-wave and measurement results.**

***Index Terms*—Bessel beams, leaky waves, near-field focusing, resonant cavities, wireless power transfer.**

I. Introduction

The possibility to focus the electromagnetic energy in a narrow spatial region and to limit its diffractive spreading has a great interest for many practical applications. These features are fulfilled by a specific class of solutions of the Helmholtz equation called *localized waves* [1], [2]. The main common characteristic of localized waves is their theoretically *diffraction-free* behavior.

Among localized waves, the simplest yet the most known solutions are *Bessel beams* (BBs) [3]. They simultaneously show a limited-diffractive, focusing, and self-healing behavior, i.e., they are able to maintain their localized transverse profile over large distances and can regenerate themselves after an obstacle placed along their propagation axis [4]. Thanks to these intriguing features, BBs have been investigated as a next-generation solution in many practical scenarios, such as near-field point-to-point communications [5], imaging [6], and, recently, wireless power transfer (WPT) [7]–[12].

Devices able to generate BBs at microwaves and millimeter (mm) waves are typically referred to as *BB launchers*. Although they exist in different architectures (see, e.g., [8], [13]–[22]), here we focus on *resonant* BB launchers based on higher-order leaky waves only [11], [18], [23], as they offer an efficient, low-profile, cost-effective, and compact solution, suitable for WPT scenarios.

In the literature, dielectric-filled launchers have been considered due to the easier physical implementation with respect to *air-filled* launchers. The latter are however preferable in order to reduce the dielectric losses that may become unbearable as the working frequency increases, at least with common low-cost materials [23]. On the other hand, an air-filled cavity requires a thorough analysis and poses more challenges in terms of fabrication. In this work, air-filled BB launchers have been designed and, for the first time, fabricated and experimentally validated. A circular aluminum ring has been conceived to precisely connect and align the feeding network with the launcher, consisting of an isotropic metasurface. The latter has been realized using a thin, yet rigid, tungsten sheet.

A key feature of the BBs considered in this paper is their polarization. Most of the previous studies on BBs, both of the wideband and of the resonant kind, deal with devices excited by coaxial feeders. The latter can effectively be modeled as vertical electric dipoles (VEDs); hence, the resulting BB has a transverse-magnetic (TM) polarization. By duality, a transverse-electric (TE) polarized BB launcher could be excited by a vertical magnetic dipole (VMD), whose

Manuscript submitted June 13, 2024. This work was partly funded by the Italian Ministry of Education, University and Research (MIUR) within the framework of the PRIN 2017-WPT4WID ('Wireless Power Transfer for Wearable and Implantable Devices') project. The work of A. Costanzo and F. Benassi was partially funded by the European Union (EU) under Italian National Recovery and Resilience Plan (NRRP) of NextGenerationEU, partnership on "Telecommunications of the Future" (Program RESTART) under Grant PE00000001 – Spoke 7.

F. Benassi, G. Paolini, D. Masotti and A. Costanzo are with the Department of Electrical, Electronic and Information Engineering Guglielmo Marconi (DEI), University of Bologna, Bologna, Italy (e-mail: francesca.benassi9@unibo.it; giacomo.paolini4@unibo.it; diego.masotti@unibo.it; alessandra.costanzo@unibo.it)

E. Negri, P. Burghignoli and A. Galli are with the Department of Information Engineering, Electronics and Telecommunications (DIET), Sapienza Univeristy of Rome, Rome, Italy (e-mail: edoardo.negri@uniroma1.it; paolo.burghignoli@uniroma1.it; alessandro.galli@uniroma1.it).

W. Fuscaldo and F. Maita are with the Istituto per la Microelettronica e Microsistemi (IMM), Consiglio Nazionale delle Ricerche, Rome, Italy (e-mail: walter.fuscaldo@cnr.it; francesco.maita@cnr.it).

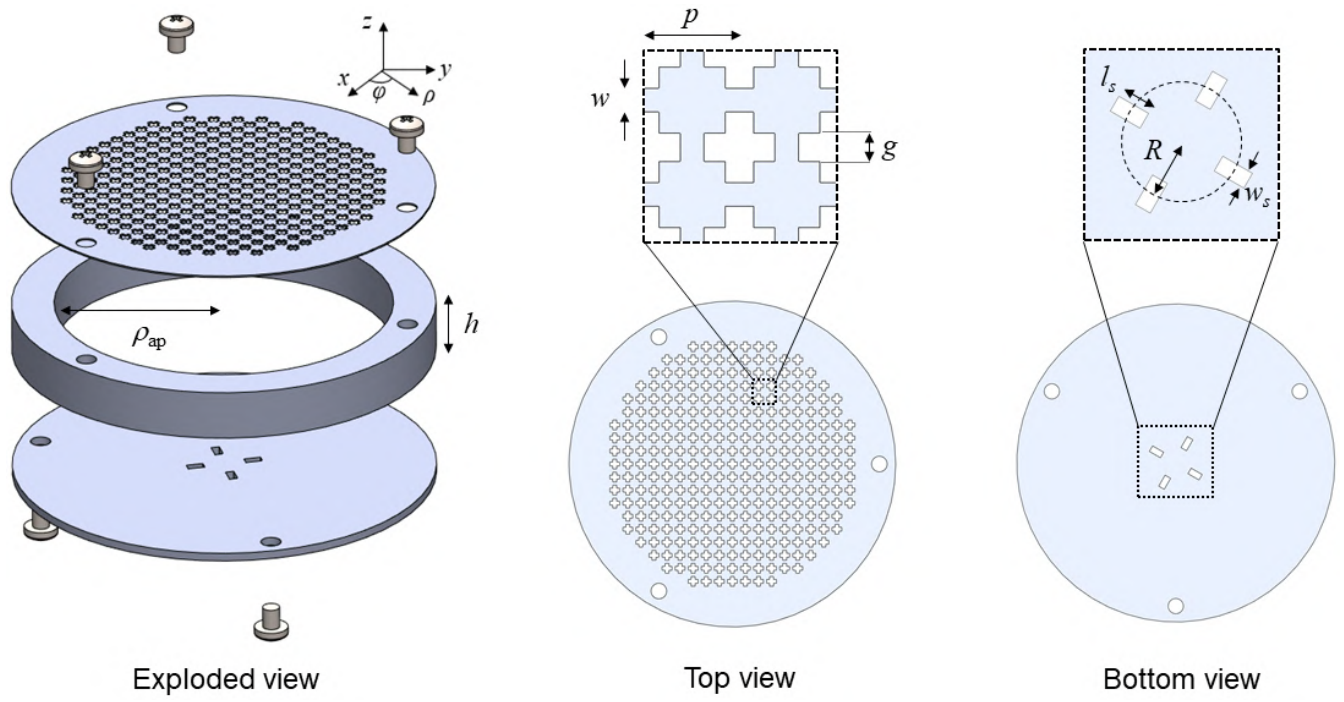

Fig. 1. Exploded, top, and bottom view of the proposed TE-polarized resonant BB launcher along with its relevant geometrical parameters. The device is fed through an array of four radial slots on the ground plane (see the bottom view) and it is constituted by a metallic cavity whose upper plate is replaced by a PRS. The latter has been implemented through a fishnet-like metasurface (see the top view).

physical implementation is however far from being trivial. In fact, the physical counterpart of VMDs is usually given by loop antennas or feeding coils [20], [21], but their feeding point breaks the azimuthal symmetry inside the cavity, thus producing a *hybrid* TE (HTE) [24], rather than a *pure* TE, polarization [25] for the propagating BB. These spurious TM components are further enhanced by the resonant conditions inside the cavity and their effect is thus more prominent with respect to loop antennas radiating in free space [24].

The implementation of a TE-polarized BB launcher has a crucial importance both from a theoretical and a practical viewpoint. As shown in [20], the excitation of a TE-polarized field minimizes the coupling with lossy dielectric materials. For this reason, the possibility to excite a *pure* TE-polarized field through a resonant BB launcher has recently and preliminarily been investigated. In [23], the excitation of a TE-polarized leaky-wave mode has been achieved through a circular waveguide feeder operating on the azimuthally symmetric higher-order TE_{01} propagation mode. Such a feeder excites a pure TE-polarized BB but needs a bulky feeding network to isolate the desired higher-order mode in the circular waveguide [26]–[28]. Another possibility has been shown in [25] where a *pure* TE-polarized BB has been obtained through the ideal, simultaneous, in-phase excitation of a circular array of $N = 8$ radial slots. Here, in order to achieve a practical demonstrator of an air-filled TE-polarized BB launcher, the number of slots is reduced to $N = 4$ to implement an innovative and realistic feeding scheme for this kind of structures (and not just the ideal simultaneous excitation of slots preliminary investigated in [25] and theoretically studied in [29]). Results in Sec. III will demonstrate that with four slots a high polarization purity is maintained.

In this regard, a meandered microstrip network is here proposed as an original feeder for a TE-polarized BB launcher able to ensure a uniform excitation of the four slots both in amplitude and in phase. At mm-wave frequencies the feeding structure is highly sensitive to losses related to meandered arrangements, thus the design must be carried out by means of combined geometric and electromagnetic optimizations to find the best and most accurate trade-off between a precise geometrical arrangement and a correct radiofrequency (RF) signal distribution. The exciting structure design is shown from a theoretical and practical viewpoint obtaining an excellent performance and good matching between simulated and measured results.

Moreover, the designed launchers are exploited in a radiative near-field WPT scenario. The importance of radiative near-field WPT links has been recently investigated in [30] and [25], showing how such links outperform typical reactive near-field [31] and far-field [32] WPT links in terms of working distance and efficiency, respectively [10]. In this work, the WPT performance is reported in terms of link budget and it is evaluated through a fast semi-analytical numerical method. The results expected from the proposed accurate method are corroborated by the first experimental validation of a radiative near-field link among resonant BB launchers and the evaluation of the link performance in a realistic environment.

The paper is organized as follows. Sec. II shows the design workflow of a TE-polarized resonant BB launcher through a simple yet powerful leaky-wave approach, whereas Sec. III describes the implementation of a realistic feeding network.

In Sec. IV, the link budget estimation in a WPT scenario is carried out for two TE-polarized BB launchers, fabricated and validated by the measurement campaign as shown in Sec. V. Conclusions are finally drawn in Sec. VI.

II. Theoretical design workflow

In this Section, the theoretical design of a TE-polarized resonant BB launcher is presented through an efficient leaky-wave approach in order to introduce the physical implementation of the feeding network and of the device described in the subsequent Secs. III and V-A, respectively.

As mentioned in the Introduction, resonant BB launchers are low-cost, compact, and effective devices capable of focusing electromagnetic energy in a narrow spatial region at microwaves and mm waves. As shown in Fig. 1 (a reference coordinate system $\{\rho, \phi, z\}$ is used hereafter), they are typically constituted by a cylindrical metallic cavity excited by a dipole-like source whose upper plate is a partially reflecting sheet (PRS) which enables the power to *leak*, and then radiate, while propagating [17], [18]. For this reason, this kind of structures can effectively be described by the straightforward, yet powerful and rigorous theoretical leaky-wave approach [11], [17], [18], [33].

Regardless the polarization type, a constructive interference between an *outward* cylindrical leaky wave generated by the source and an *inward* one reflected back by the circular metallic boundaries has to be enforced to obtain a limited-diffractive BB distribution. From a practical viewpoint, both amplitude and phase constraints have to be ensured to maintain almost the same amplitude for the outward and the inward contributions and to ensure the vanishing of the electric-field tangential components on the metallic rim, respectively [17].

The first condition can be satisfied by enforcing a design constraint on the *attenuation* (or *leakage*) *constant* α, i.e., the imaginary part of the leaky-wave radial wavenumber $k_\rho = \beta - j\alpha$ (being β the *phase constant*). As shown in [23], it is possible to achieve a good representation of a BB distribution through an inward and outward cylindrical leaky wave if approximately $\alpha \leq 0.03/\rho_{\rm ap}$, being $\rho_{\rm ap}$ the *aperture radius*, i.e., the inner radius of the cylindrical cavity.

Once the amplitude condition is enforced through the attenuation constant value α, the phase condition has to be applied through the leaky-wave phase constant β. In particular, the tangential electric-field components must vanish on the circular metallic rim, thus obtaining a different resonant condition for each polarization. In an ideal TE-polarized BB launcher, a zeroth-order Bessel function $J_0(k_\rho\rho)$ describes the vertical component (along the z-direction) of the electric vector potential. In such a way, the magnetic-field component H_z also follows a $J_0(\cdot)$ distribution. The transverse components, i.e., E_ϕ and H_ρ, have a radial dependence described instead by a first-order Bessel function $J_1(k_\rho\rho)$ [23]. Therefore, since the only nonzero electric-field component in an azimuthally symmetric TE field is E_ϕ, the radial resonance is enforced by equating j_{1q}, the q-th zero of $J_1(\cdot)$, to the real part of the Bessel function argument [20], [21]:

$$\beta\rho_{\rm ap} = j_{1q}. \tag{1}$$

The radial-resonance order q can be set almost arbitrarily in conjunction with the geometrical and physical parameters (e.g., frequency) of the structure. The first radial resonance, however, is typically avoided due to the occurrence of undesired non-negligible truncation effects. For this reason, the second radial resonance, i.e., $q = 2$, is assumed in the following in order to achieve a more compact device and the minimum number of secondary lobes [10]. The working frequency f_0 is chosen depending on practical constraints, such as usable bands and dimension limits. An additional practical restriction depending on the specific application target is given by the device size. We are here interested to rather miniaturized WPT devices, so that the maximum aperture radius of the launcher is fixed at $\rho_{\rm ap} = 2$ cm, considering an additional margin of 0.5 mm to physically implement the circular metallic rim (see Fig. 1).

In order to excite a leaky-wave mode with the desired β and α values at the working frequency f_0 and with a fixed value for the aperture radius, the effect of the cavity height h and the specific PRS has to be studied through a transverse-resonance-technique (TRT) approach (see, e.g., [11] and references therein). The TRT is applied to the transverse equivalent network of the cavity in order to obtain the dispersion equation of the relevant TE-polarized leaky mode. The dispersion equation is then numerically solved for the complex improper roots in order to find the leaky wavenumber [34].

In this context, a PRS constituted by a lossless, isotropic, homogenized metasurface is simply represented through a purely imaginary sheet impedance $Z_{\rm s} = jX_{\rm s}$, being $Z_{\rm s}$ the equivalent surface impedance and $X_{\rm s}$ its imaginary part (reactance). As shown in [35], typical two-dimensional (2-D) metal arrangement, such as patch arrays, metal strip gratings, or fishnet-like metasurfaces can efficiently and rigorously be described in this way.

The cavity height h and $X_{\rm s}$ are strictly related to each other and they can be found, as shown in [36], in order to obtain the desired values of α and β at the working frequency f_0. While h is simply set by the metallic-cavity inner height (see Fig. 1), the equivalent PRS surface impedance has to be implemented through a homogenized metasurface topology with specific physical dimensions.

In this work, an inductive PRS is used, constituted by a fishnet-like metasurface whose design parameters, shown in Fig. 1, are: the unit-cell period p, the strip width w, and the patch gap g [35]. It is worth noting that the period p has to be selected in order to work under the homogenization limit, i.e., $p \ll \lambda_0$ (being λ_0 the vacuum wavelength at the working frequency f_0).

The characterization of the fishnet-like metasurface and the evaluation of its equivalent $X_{\rm s}$ value have been performed as shown in [35]. In particular, in order to obtain the desired $X_{\rm s}$ value, the unit-cell design parameters p, w, and g reported in Table I are used. It is worth pointing out that, differently from [35] where an ideal zero-thickness perfect electric conductor (PEC) is considered, the fishnet-like metasurface is here realized and designed assuming a realistic tungsten sheet. Since an isotropic PRS can be described in terms of a simple

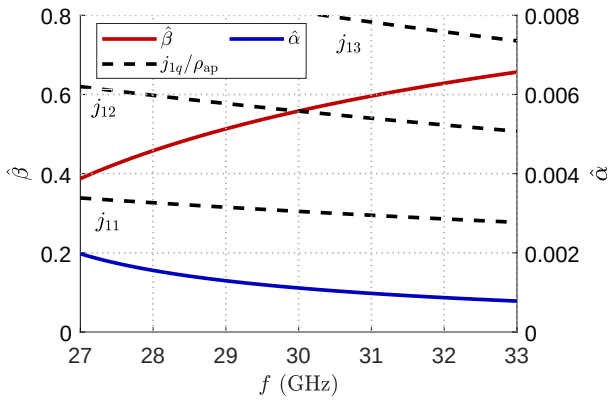

Fig. 2. The dispersion curves of the leaky-wave phase (β) and attenuation (α) constants, normalized with respect to the vacuum wavenumber k_0, are reported as $\hat{\beta} = \beta/k_0$ and $\hat{\alpha} = \beta/k_0$ through a red and a blue solid line vs. frequency f for a structure with parameters as in Table I, respectively. The radial resonance curves of the $q = 1, 2, 3$ zeros of the first-order Bessel function of the first kind, $J_1(\cdot)$, are reported through black dashed lines.

sheet impedance only if it is electrically thin, a very low-profile metal arrangement was necessary. For this reason, a 0.2 mm (corresponding to $\lambda_0/50$) thick fishnet-like metasurface has been realized through a tungsten sheet which simultaneously shows a very high conductivity (namely $\sigma = 1.76 \cdot 10^7$ S/m), rigidity, and planarity. Further details can be found in Sec. V.

As shown in Fig. 2, where the dispersion curves of the normalized phase $\hat{\beta} = \beta/k_0$ and attenuation $\hat{\alpha} = \alpha/k_0$ constants, being k_0 the vacuum wavenumber, are reported vs. frequency f, the second radial-resonance curve for TE modes [given by (1)] intersects the normalized phase-constant dispersion curve exactly at the desired working frequency $f_0 = 30$ GHz. Moreover, as expected, the normalized attenuation constant values $\hat{\alpha}$ are sufficiently small to ensure the abovementioned amplitude condition. These curves have been achieved by considering the design parameters $\rho_{\rm ap}$, h, and $X_{\rm s}$ in Table I.

The evaluation of the leaky phase constant is not only important for the correct design of the device and to have a vanishing azimuthal electric field on the metallic boundaries, but also for the evaluation of the *nondiffractive range* (ndr). The nondiffractive range indicates the maximum distance from the aperture plane for which the truncated BB, i.e., the BB generated by a realistic, finitely extended aperture, remains approximately propagation invariant. As shown and corroborated in previous works (see, e.g., [23] and references therein), the nondiffractive range can be computed through the ray-optics approximation, as [3]:

$$z_{\rm ndr} = \rho_{\rm ap} \cot \theta_0, \tag{2}$$

being θ_0 the so-called *axicon angle*. The latter is strictly related to the leaky-wave phase constant through the relation $\beta = k_0 \sin \theta_0$ [17]. Since in this case, at the working frequency $f_0 = 30$ GHz, we have $\beta \simeq 0.56 k_0$, it results that $\theta_0 \simeq 34^\circ$ and $z_{\rm ndr} = 29.7$ mm.

The last design step is related to the realistic feeder implementation. As discussed in the Introduction, TE-polarized BB launchers are indeed not common in the available literature due to the problems related to realistic implementations of VMDs through electric current loops. In order to avoid the need of shifting the loop position to partially limit the occurrence of TM contributions as in [20], in [25] a radial 8-slot array on the ground plane has been considered as the discrete counterpart of a continuous azimuthally symmetric radially directed magnetic surface current, which is transversely irrotational and, by reciprocity, excites an irrotational transverse magnetic field, i.e., a TE-polarized field. Although a higher number of slots would better approximate such an ideal surface current, only four slots have been considered in this work in order to achieve a physically realizable design, nonetheless obtaining high polarization purity, as shown next. The design parameters of the slots, pictorially represented in Fig. 1, are reported in Table II. How these slots have been excited, the original feeding network design, and its implementation are the topics addressed in the following Sec. III.

III. Feeding Network Design

In this Section, a realistic network in microstrips technology is designed to ensure identical slots excitation, both in amplitude and phase. In a first stage a 4-port microstrip network, with the ground plane coincident with the BB-launcher bottom metal plane hosting the slots, has been considered. It consists of four identical open stubs to excite the slots, designed to provide a 50-Ω impedance at each port. To obtain an irrotational transverse magnetic field, a prescribed mutual orientation between each slot-feeding line pair must be ensured. Starting from this 4-port network [see Fig. 3(a)], a 5-port network has been designed to be finally connected to the first one, by means of the sub-network growth method [37]. The resulting 1-port network has been optimized by carefully taking into account and maintaining as much as possible the symmetry conditions mentioned before: on one hand, the symmetry forces a meandering arrangement of the feeding branches, requiring a more accurate tuning especially due to the operating frequency of 30 GHz; on the other hand, it allows for initially designing only one half of the structure. The first step of the optimization process has been to characterize the mutual coupling of the four slots in the presence of the upper cavity equipped with the fishnet-like PRS in terms of a 4-port network, whose terminal planes are located on the microstrips feeding the slots in proximity of the latter. This computation is carried out by means of full-wave simulations and the relevant setup is shown in Fig. 3(a).

This characterization allows us not only to quantify the impedance to be matched by the feeding network, but also it is of paramount importance to take into consideration the

TABLE I
Design Parameters of a TE-Polarized BB Launcher Working at 30 GHz

$\rho_{\rm ap}$ (mm)	h (mm)	$X_{\rm s}$ (Ω)	p (mm)	w (mm)	g (mm)
20	5.92	24.23	2	0.5	0.6

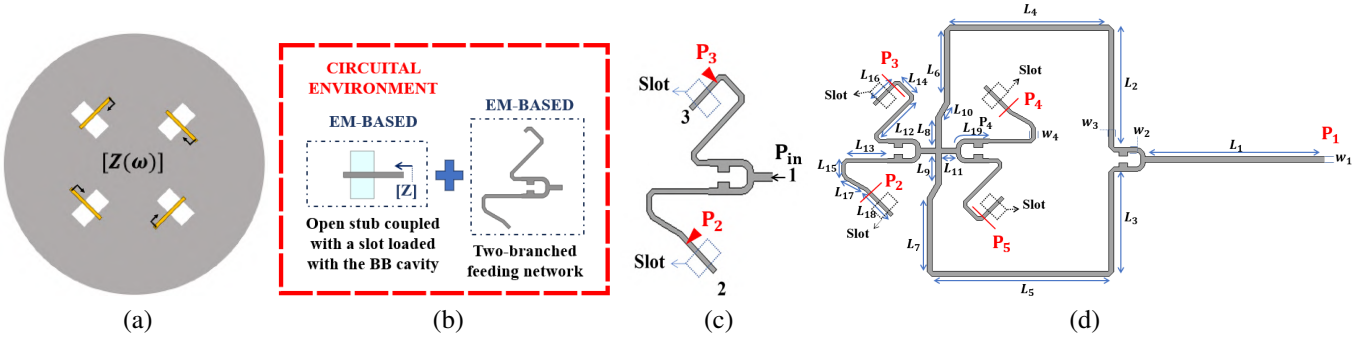

Fig. 3. (a) Schematic view of the full-wave characterization of the 4-port network used as load of the design feeding network. (b) Illustrative representation of the blocks designed by means of full-wave simulations. (c) Rendering of a portion (one half) of the designed feeding network, highlighting the geometrical arrangement of the branches. (d) View of the designed feeding network. The slot positions are represented for reference with dotted lines. Dimensions, in mm, are: $L_1 = 12.27$, $L_2 = 7.47$, $L_3 = 6.36$, $L_4 = 10.2$, $L_5 = 11.3$, $L_6 = 4.58$, $L_7 = 4.67$, $L_8 = 1.98$, $L_9 = 1.88$, $L_{10} = 1.1$, $L_{11} = 0.96$, $L_{12} = 3.15$, $L_{13} = 2.6$, $L_{14} = 1.2$, $L_{15} = 0.72$, $L_{16} = 1.95$, $L_{17} = 1.5$, $L_{18} = 2.3$, $L_{19} = 2.1$, $w_1 = 0.35$, $w_2 = 0.3$, $w_3 = 0.35$, and $w_4 = 0.23$.

TABLE II
PARAMETERS OF RADIAL SLOT FEEDING

Parameter	R	l_s	w_s
Value (mm)	3.5	2	1

possible existing coupling between the slots. The goal of the optimization process is to have a feeding signal that has the same amplitude and phase in the same section of all the four branches feeding the slots. This purpose, combined with geometrical and orientation constraints in a mm-wave operative context, forces the design to be carried out by full-wave simulations. Each slot must be fed by one branch of the feeding network that needs not only to be compliant with the slot orientation, as can be inferred from Fig. 3(a), but must also be of the same electrical length in order to be able to provide a signal with the same amplitude and phase. To reduce the computational time, and also to find a starting point from which to conduct a combined geometrical/electromagnetic optimization, two of the four branches of the feeding network are modeled and optimized, as schematically represented in Fig. 3(b) and Fig. 3(c). We should stress that the extracted 4-port network cannot be directly connected to the two-branch designed feeding network, thus the specific value of impedances for the operating frequency are extracted directly from the full-wave simulator and used for a preliminary rough performance evaluation. The complex impedances calculated in the sections of the lines immediately before slots 2 and 3, [P_2 and P_3 in Fig. 3(c)] are: $17 - j78\ \Omega$ and $16 - j70\ \Omega$, respectively, and they are used as load terms for the two branches simulated network.

Because these impedances are complex, the modeling and optimization of the power divider should follow design steps as in [38]. However, the challenge added to this design is strongly related to the geometrical arrangement of the structure, implying the choice of carrying out the design by means of full-wave simulations.

To evaluate the performance of this branch in terms of power distribution, the RF-power provided at each slot [P_2 and P_3 in Fig. 3(c)], when a 27 dBm input power is provided to the input port, [P_1 in Fig. 3(d)], has been first evaluated through a circuital simulator that combines the two full-wave blocks, as in Fig. 3(b). After a fine tuning of the branch length, enabled by the use of a circuital simulator, the obtained results are reported in Table III, showing an equal distribution of the signal between the two branches, both in terms of amplitude and phase.

TABLE III
SIGNAL DELIVERED TO EACH PORT AT 30 GHZ
(2-BRANCH FEEDING NETWORK)

	Mag. (dBm)	Phase (°)
P_2	22.98	39.3
P_3	22.83	38.4

The combined full-wave/circuital simulation enables the tuning of the feeding network with the aim of finding the best trade-off among system performance, in terms of power splitting, dimensions, and orientation arrangement constraints introduced by the slot-fed type of feeding. Authors are aware that the choice of using the extracted fixed values of impedances as loads of the feeding network introduces an approximation of the overall behavior of the network, because the mutual influence and coupling between the two ports, and between each port and the others, is not accounted for. However, it gives a useful starting point, especially in terms of geometrical arrangement, to conduct the final optimization of the overall structure. After validating the feasibility of a design having two branches, the final feeding network is realized exploiting the perfect radial symmetry of the system, resulting in the arrangement shown in Fig. 3(d).

Now that the feeding network is equipped with four symmetrical branches, in order to provide the input signal correctly, two additional branches are introduced for compensation purposes. In fact, a single microstrip line feeding the 4-branch structure would introduce a small coupling between the two slot-fed sections in close proximity, modifying not only the power distribution but also the phase shift in each branch. The final optimization of the entire network accounts for the combination of the 4-port system,

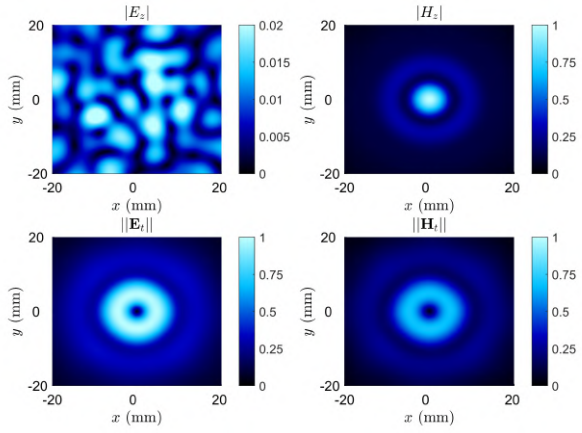

(a)

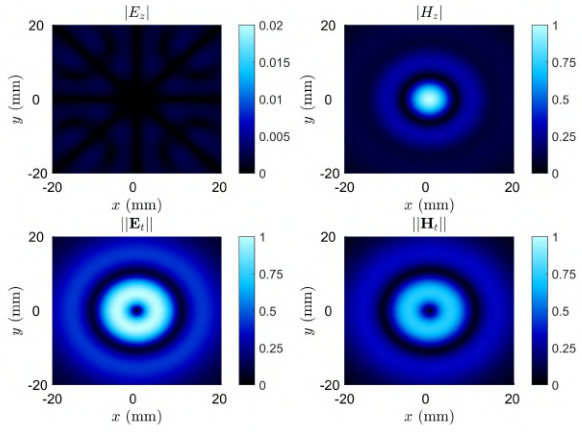

(b)

Fig. 4. Full-wave outcomes for the (a) TE-polarized launcher with the proposed optimized feeding network and (b) with the ideal radial slot array. Both field distributions are reported on an xy-plane at $z = 12$ mm.

modeling the impedance offered to the feeding network by the presence of the BB cavity, with the 5-port network as in Fig. 3(d). The optimization process, carried out in a circuital environment has led to the final arrangement shown in Fig. 3(d). This process allows us to verify not only the overall tuning of the system, with the center frequency at 30 GHz, in agreement with the full-wave simulations of the entire structure, but also to validate the correct power distribution at each port, namely P_2, P_3, P_4 and P_5. Table IV lists the power delivered to each of the four slots when a 27 dBm input power is provided to the feeding network input port [see Fig. 3(d) for reference].

It is worth mentioning that both the high operating frequency and the meandered structure forced by the need of achieving symmetry introduce some losses in the overall power distribution leading to resulting values that slightly differ from the theoretical ones.

After the feeding network has been numerically simulated and optimized, the final geometrical parameters, reported in the caption of Figs. 3, are used as a source for the designed BB launcher. A full-wave simulation of the entire structure has been carried out in CST Microwave Studio [39] to verify the effectiveness of this excitation scheme, when compared to the same launcher excited by a radial slot array. As shown in Fig. 4, the field distribution computed for an operating distance of 12 mm from the radiating aperture is in agreement with the expected results. To ease the comparison and visualization of the TE polarization, the electric field components are normalized with respect to the maximum value of the transverse electric field component $||\mathbf{E}_t||$ on the $z = 12$ mm plane and the magnetic ones are normalized with respect to the maximum value of H_z. As can be inferred from Fig. 4, the tangential components $\mathbf{E}_t$ and $\mathbf{H}_t$ have a radial dependence described by a $J_1(\cdot)$ function, whereas the longitudinal component H_z follows a $J_0(\cdot)$ profile, as expected. The proposed launcher experiences an E_z component that is 16 dB lower than $||\mathbf{E}_t||$, whereas, in the *hybrid-TE* polarized BB launcher presented in [24] the E_z component is only 10 dB lower than $||\mathbf{E}_t||$. Indeed, the solution exploiting the 4 radial slot array, fed ideally with discrete ports, would allow for obtaining an E_z component that is 30 dB lower than $||\mathbf{E}_t||$ [see Fig. 4(b)] and, therefore, a *pure* TE-polarized BB. However, the unfeasibility of this solution makes it simply a gold standard, whereas the final results, shown in Fig. 4(a), confirm that the designed structure represents a valid feeder for a TE-polarized BB launcher, improving the results obtained in [24]: actually a high polarization purity is maintained (having a still negligible contribution of E_z), thus obtaining a realistic implementation of a TE-polarized BB.

IV. Link Budget Estimation

After carrying out the design and verification of the customized matched feeding network loaded by the cavity, a link budget estimation is performed to quantify the system performance in terms of wireless power transmission. The general-purpose link-budget numerical approach, extensively described in [40], is exploited and applied considering two slot-fed TE-polarized BB launchers as transmitting (TX) and receiving (RX) antennas. This approach allows for obtaining an accurate link budget calculation without the need of simulating an entire WPT link made of two launchers in an electromagnetic environment. The full-wave characterization of a single launcher, carried out by means of CST Microwave Studio [39], provides the electromagnetic field components that are extracted, numerically post-processed, and used by a custom-made numerical algorithm based on [40]. In particular, the collected electromagnetic fields are both analyzed on a surface S that is located between the two launchers. The

TABLE IV
Signal delivered to each port at 30 GHz
(4-branch feeding network)

	Mag. (dBm)	Phase (°)
P_2	20.2	51.2
P_3	20.2	51.0
P_4	20.7	57.7
P_5	20.2	55.7

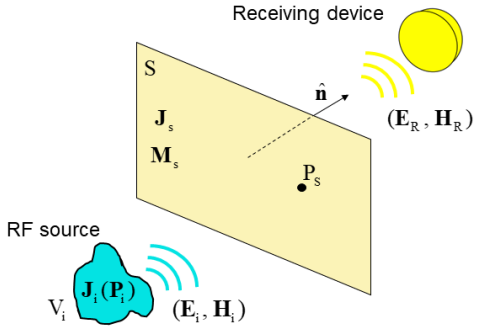

Fig. 5. Model based on the electromagnetic theory for quick and precise link-budget evaluation.

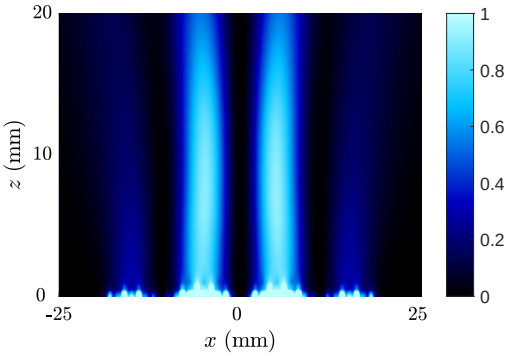

Fig. 6. Plot of the equivalent current density normalized with respect to its maximum for an xz plane.

assessment plane is positioned in the center of the separation space between the two launchers in the scenario, as depicted in Fig. 5.

By combining the reciprocity and equivalence theorems, this technique enables the representation of the receiving device through a Norton equivalent circuit, whose current source is $I_{\rm eq}$. Through full-wave simulations, the receiving antenna admittance $Y_{\rm a}(\omega)$ may be assessed, which reduces the computation of the received power to the assessment of $I_{\rm eq}$ in the presence of a monochromatic incident field from a transmitting antenna with volume $V_{\rm i}$. The reciprocity theorem can be used to make the receiving antenna switch between operating in the transmitting mode (while being driven by a sinusoidal voltage source with an internal impedance of $Z_{\rm R}$ and electromotive force U), and in the receiving mode (while being loaded by $Z_{\rm R}$ and illuminated by the incident field produced by the transmitting antenna). The independent transmitting antenna of volume V_i is replaced by the electric and magnetic surface currents $\mathbf{J}_{\rm s}$ and $\mathbf{M}_{\rm s}$ depicted in Fig. 5, computed on the plane S, to simulate a two-antenna connection and expand these calculations to a generic situation involving both far- and near-field conditions. Subsequently the Norton current $I_{\rm eq}$ can be precisely computed as follows (see Fig. 5):

$$I_{\rm eq} = \frac{1 + Z_{\rm R} Y_{\rm a}(\omega)}{U} \hat{\mathbf{n}} \cdot \int_S [\mathbf{E}_{\rm i}(P_{\rm S}) \times \mathbf{H}_{\rm R}(P_{\rm S}) - \mathbf{E}_{\rm R}(P_{\rm S}) \times \mathbf{H}_{\rm i}(P_{\rm S})] {\rm d}S \quad (3)$$

where $\mathbf{E}_{\rm i}$, $\mathbf{H}_{\rm i}$, $\mathbf{E}_{\rm R}$ and $\mathbf{E}_{\rm R}$ are the electric and magnetic fields of the transmitting and receiving BB launchers, respectively.

The received power can then be computed as [41]:

$$P_{\rm r} = (1/8)|I_{\rm eq}|^2 / {\rm Re}\left[Y_{\rm a}(\omega)\right] \quad (4)$$

where $Y_{\rm a}(\omega)$ is the internal complex admittance of the considered antenna, i.e., the TE-polarized BB launcher. As it can be inferred from (4), the correct computation of $I_{\rm eq}$ allows for safely estimating the overall link power budget. In particular, from the equation for $I_{\rm eq}$, reported in [40], it is possible to plot the equivalent current density in the longitudinal xz plane at $y = 0$, by computing the integrand of such equation. In this manner, as shown in Fig. 6, it is possible to notice that, as expected, it has a zero in the center of the aperture, in agreement with the distribution of the transverse components of the fields that follows a $J_1(\cdot)$ profile [23]. The link power budget has been subsequently computed for different operating distances between the two launchers: 20, 30, and 40 mm, respectively in order to enable a fair performance comparison with previous works.

The received power levels for the three considered distances are reported in Table V together with the power levels presented in [25] to perform a safe comparison between the proposed solution and the previous designs, which are computed considering an input power of 27 dBm. For the sake of completeness, the results obtained for the shortest distance of 20 mm exploiting the proposed method have been compared with full-wave simulations, obtaining $|S_{21}|$ values of -10.60 dB and -10.05 dB respectively. This comparison is of paramount importance to show that coupling effects do not modify significantly the transmission coefficient over the frequency of interest.

TABLE V
RECEIVED POWER AT 30 GHZ FOR TE-POLARIZED BB LAUNCHERS WITH AN IDEAL OR A REALISTIC FEEDER FOR DIFFERENT WORKING DISTANCES

TX-RX distance (mm)	$P_{\rm r}$ (dBm) Radial slot (ideal) [25]	$P_{\rm r}$ (dBm) **TE (this work)**
20	19.6	**16.4**
30	15.4	**12**
40	12.5	**8.8**

V. EXPERIMENTAL VALIDATION

In this Section V, the fabrication process of an original air-filled millimeter-wave resonant BB launcher is presented. The designed radiating device and its feeding network is then experimentally validated. Moreover, a measurement campaign of a WPT link between two BB launchers is addressed for the first time for three different distances, namely 25, 35, and 48 mm.

A. Fabrication process

Prototypes have been fabricated through a combination of machining processes, involving the utilization of computer numerical control (CNC) milling and laser cutting, to assemble three distinct components according to the design shown in

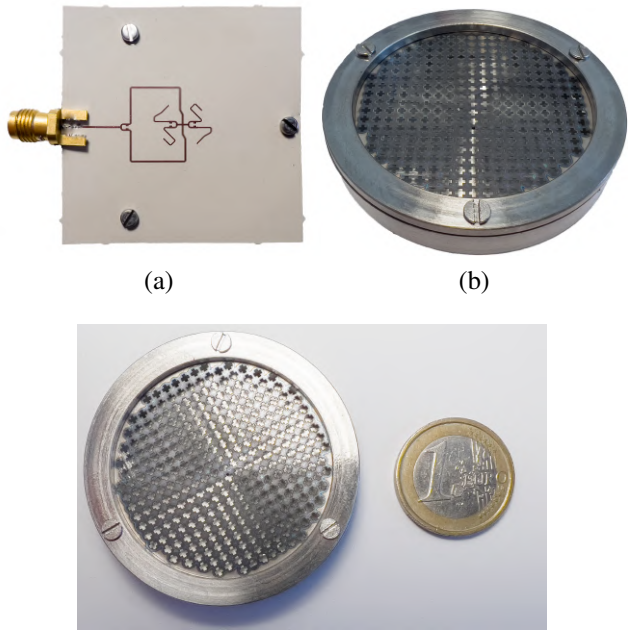

Fig. 7. (a) Picture of the realized feeding network, equipped with anchor holes on the substrate; (b) the realized BB launcher; and (c) a comparison of the realized BB launcher with a 1 euro coin.

the exploded view of Fig. 1. Specifically, the hollow cylinder, fabricated from aluminum through CNC milling, features a 5 mm-thick frame, essential for accommodating the securing screws for the other two elements. The screw holes were strategically arranged in two groups of three, spaced 120 degrees apart on both the upper and lower planes, ensuring the utmost planarity of the object. For the lower part, the feeding-network printed circuit board (PCB), connected to the device through the three bottom screws, also acts as the slotted ground plane. On the other hand, crafting the upper part with the fishnet pattern required a more delicate approach. A laser cutting technique was precisely operated on a 0.2-mm thick tungsten sheet. The use of tungsten was crucial to maintain material rigidity and planarity in spite of the reduced thickness, which is a feature required to minimize losses and to properly represents the PRS as a purely imaginary sheet impedance. In order to further enhance precision during fabrication, the cutting process was conducted in steps rather than all at once. This approach effectively mitigated the detrimental effects of thermal and mechanical stress on the delicate fishnet structure.

B. Measurement results

After carrying out an accurate optimization process, the prototype has been fabricated (Fig. 7) and measurement campaigns have been conducted. First, the feeding network has been realized accounting for the presence of holes for anchor purposes. A close-up of the feeding network is shown in Fig. 7(a).

The reflection coefficient of the presented feeding network is measured by means of a vector network analyzer (VNA) without the presence of the BB launcher and results are

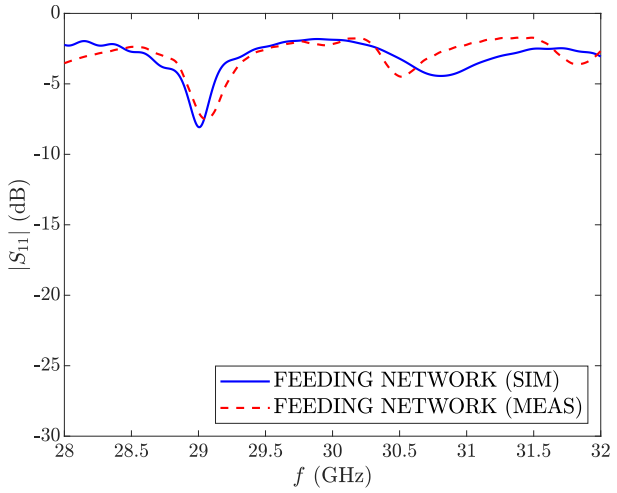

Fig. 8. Simulated and measured reflection coefficient in absolute value (in dB) for the proposed feeding network.

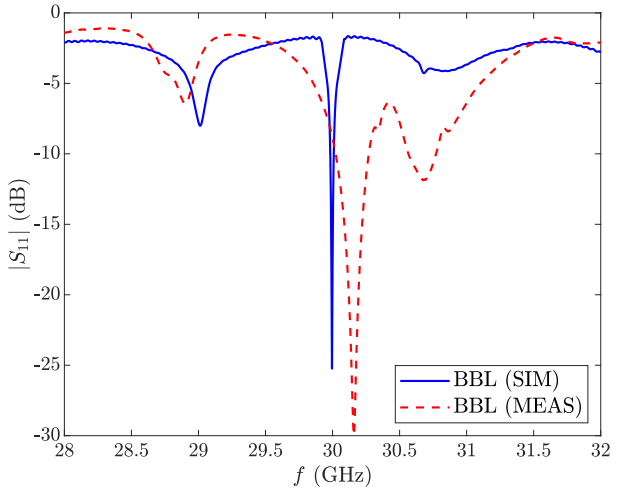

Fig. 9. Simulated and measured reflection coefficient in absolute value (in dB) for the proposed TE-polarized BBL.

compared with simulated ones. As can be inferred by Fig. 8, the characterization of the feeding network is carried out in a frequency range from 28 to 32 GHz, showing good agreement with the simulations. Minimal discrepancies among simulated and measured results are possibly related to some imperfections in the physical implementation of the device and they can be considered negligible. As expected, the feeding network without the presence of the cavity approximately behaves as if it were terminated on an open circuit, hence different from the load for which it had been optimized, thus it does not show good impedance matching around the resonant frequency. However, such a characterization allows to validate the feeding part of the system to better confirm the overall system performance. Subsequently, the entire system is assembled and fixed exploiting other three screws located on the bottom layer in order to firmly close the cavity and allow the feeding-network PCB. The reflection coefficient at the system input port is then measured. Simulated and measured results are compared and plotted in Fig. 9.

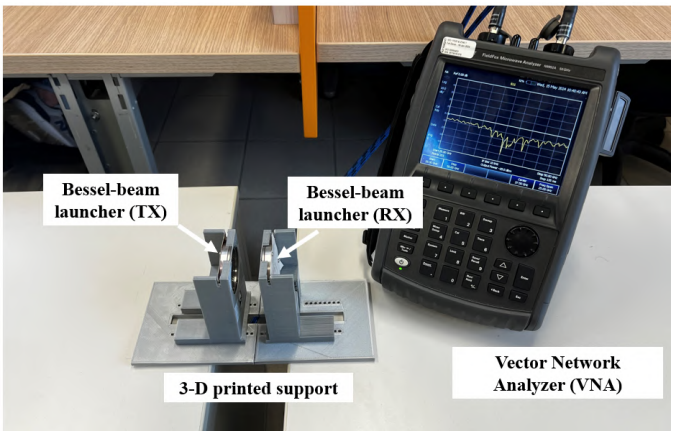

Fig. 10. Photo of the measurement setup. A 3D-printed structure is realized for holding the launchers and the scattering parameters of the link are measured using a VNA.

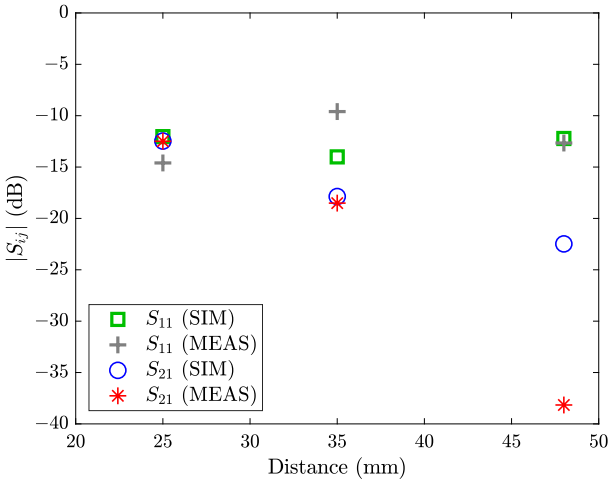

Fig. 11. Simulated and measured S-parameter results in absolute value (in dB) for a link configuration of two TE-polarized BB launchers in a real-world scenario for an increasing separation distance, namely 25, 35, and 48 mm.

Measurements and simulations of $|S_{11}|$ are in fair agreement. The main difference is related to a shift of the measured resonance frequency which is most likely due to a difference between the simulated cavity height and the actual one, since resonant BB launchers are very sensitive to this parameter (see, e.g., [23] and references therein).

Subsequently, a link between two TE-polarized BB launchers is established and characterized. Given the high operating frequency, the measurement setup must be accurately calibrated and firmly fixed to avoid inaccurate data. Figure 10 shows the measurement setup accounting for a 3-D printed support structure to hold the launchers during the measurements. When measuring the transmission coefficient of the link, three additional distances, with respect to those in Table V, have allowed to measure the performance with a rather stable setup, especially as concerns the movement of the cables connecting each BB launcher to the VNA, and in specific interesting working conditions. Such distances are 25, 35, and 48 mm, and they have been chosen in order to place the RX launcher within the, in proximity of, and far from the nondiffractive region of the transmitting device ($z_{\mathrm{ndr}} \simeq 30$ mm), respectively. Absolute values of the measured and simulated S-parameters of an equivalent two-port network constituted by the two launchers are shown in Fig. 11. For every working distance, there is a fair agreement among the S_{11} results, always ensuring an efficient matching condition despite the TX-RX near-field coupling effect. Moreover, for a distance of 25 mm and 35 mm, simulations and measurements of the transmission coefficient are in excellent agreement, whereas the last distance, much larger than z_{ndr} (so that the received power is anyway rather reduced due to much stronger diffraction), shows a more evident discrepancy. This last result is most likely due to the greater effect of real-scenario non-idealities, mainly due to fabrication tolerances and losses, far away from the nondiffractive region of the transmitting device. Moreover, although the measurement has been conducted paying attention to the alignment of the two launchers, a slight tilt of one of the two devices may have occurred. In order to quantify the effect, full-wave simulations have been conducted showing how a simple $5°$-tilt of one of the BB launcher deteriorates the $|S_{21}|$ of about 6 dB for the highest separation distance. For the sake of completeness, Tab. VI reports the $|S_{21}|$ obtained for tilting angles spanning from $0°$ to $10°$ computed for the TX-RX distance of 48 mm. For the shorter distances no significant variations have been observed over the selected range on tilting angles.

TABLE VI
TRANSMISSION COEFFICIENTS FOR DIFFERENT TILT ANGLES FOR A TX-RX DISTANCE OF 48 MM

Tilt angle (°)	$\lvert S_{21}\rvert$ (dB)
0	-22.30
2	-22.90
5	-28.34
10	-29

It is worth pointing out that, at lower working distances, the misalignment does not impact much on the WPT performance of the devices. This effect can be simply justified considering a ray-optics approximation: since a generic tilt angle θ_{t} of a launcher with respect to the other radially shifts the beam axis of a value $\rho_{\mathrm{beam}} = z \tan\theta_{\mathrm{t}}$, the higher is the working distance of the WPT link, the farther is the beam axis from the receiver center. This possible inaccuracy, together with the non-idealities effect, has led to a significant difference between simulated and measured results appearing for the largest analyzed separation distance, which is, however, above the expected working condition of the transmitting device. The possible effects of the non-idealities on the WPT link-budget performance, especially for large distances, deserve further specific deeper investigation. Nevertheless, the obtained results aim to be a proof of concept of a design and a feasible realization of an original air-filled mm-wave TE-polarized BB launcher with a novel feeding technique to be exploited for future WPT purposes.

VI. Conclusion

In this work, an air-filled TE-polarized Bessel-beam launcher fed by four radial slots has been designed and implemented for mm-wave applications. Preliminary theoretical results have been made feasible by the design and optimization of a feeding network to enable a correct generation of an azimuthally symmetrical electromagnetic field inside the cavity. The geometrical parameters of the cavity, together with the realization of the fishnet-like metasurface, have been accurately designed, exploiting an efficient and accurate leaky-wave approach. A 30-GHz feeding network has been designed by means of a geometric and electromagnetic optimization that allows each slot to be excited with an RF-signal having the same amplitude and phase. Prototypes have been fabricated and measurement campaigns have been conducted to quantify the power transfer capabilities of the realized link. The theoretical design of such polarized BBLs has been conclusively validated by measurements in the mm-wave range that have demonstrated a reasonable agreement with full-wave simulations. The work aims to be a proof of concept of this kind of WPT technology, demonstrating the feasibility of the realized launchers and their performance in compliance with the realization process at millimeter-wave frequencies.

References

[1] H. E. Hernández-Figueroa, M. Zamboni-Rached, and E. Recami, *Localized Waves*. Hoboken, NJ, USA: John Wiley & Sons, 2007.

[2] ——, *Nondiffracting Waves*. Weinheim, Germany: John Wiley & Sons, 2013.

[3] J. Durnin, "Exact solutions for nondiffracting beams. I. The scalar theory," *J. Opt. Soc. Am. A*, vol. 4, no. 4, pp. 651–654, 1987.

[4] D. McGloin and K. Dholakia, "Bessel beams: diffraction in a new light," *Contemporary Phys.*, vol. 46, no. 1, pp. 15–28, 2005.

[5] S. Chen, S. Li, Y. Zhao, J. Liu, L. Zhu, A. Wang, J. Du, L. Shen, and J. Wang, "Demonstration of 20-gbit/s high-speed Bessel beam encoding/decoding link with adaptive turbulence compensation," *Opt. Lett.*, vol. 41, no. 20, pp. 4680–4683, Oct 2016.

[6] C. Liu, Z. Zhao, C. Jin, Y. Xiao, G. Gao, H. Xie, Q. Dai, H. Yin, and L. Kong, "High-speed, multi-modal, label-free imaging of pathological slices with a Bessel beam," *Biomed. Opt. Express*, vol. 11, no. 5, pp. 2694–2704, 2020.

[7] F. Alsolamy, W. A. Alomar, and A. Grbic, "Cylindrical vector beams for wireless power transfer," *IEEE Trans. Antennas Propag.*, vol. 69, no. 3, pp. 1716–1727, Sep. 2021.

[8] S. Paković, S. Zhou, D. González-Ovejero, S. C. Pavone, A. Grbic, and M. Ettorre, "Bessel–Gauss beam launchers for wireless power transfer," *IEEE Open J. Antennas Propag.*, vol. 2, pp. 654–663, May 2021.

[9] J. D. Heebl, M. Ettorre, and A. Grbic, "Wireless links in the radiative near field via Bessel beams," *Phys. Rev. Appl.*, vol. 6, no. 3, 034018, 2016.

[10] F. Benassi, W. Fuscaldo, D. Masotti, A. Galli, and A. Costanzo, "Wireless power transfer in the radiative near-field through resonant Bessel-beam launchers at millimeter waves," in *2021 IEEE Wireless Power Transf. Conf. (WPTC)*, San Diego, CA, USA, 2021, pp. 1–4.

[11] E. Negri, W. Fuscaldo, P. Burghignoli, and A. Galli, "Leaky-wave analysis of TM-, TE-, and hybrid-polarized aperture-fed Bessel-beam launchers for wireless power transfer links," *IEEE Trans. Antennas Prop.*, vol. 71, no. 2, pp. 1424–1436, Feb. 2023.

[12] E. Negri, L. Del Biondo, W. Fuscaldo, P. Burghignoli, and A. Galli, "Wireless radiative near-field links through wideband Bessel-beam launchers," in *53$^{\mathrm{rd}}$ Europ. Microw. Conf. (EuMC 2023)*, Berlin, Germany, 2023, pp. 1–4.

[13] M. Ettorre, M. Casaletti, G. Valerio, R. Sauleau, L. Le Coq, S. C. Pavone, and M. Albani, "On the near-field shaping and focusing capability of a radial line slot array," *IEEE Trans. Antennas Propag.*, vol. 62, no. 4, pp. 1991–1999, Apr. 2014.

[14] S. C. Pavone, M. Ettorre, M. Casaletti, and M. Albani, "Transverse circular-polarized Bessel beam generation by inward cylindrical aperture distribution," *Opt. Express*, vol. 24, no. 10, pp. 11 103–11 111, 2016.

[15] S. C. Pavone, M. Ettorre, and M. Albani, "Analysis and design of Bessel beam launchers: Longitudinal polarization," *IEEE Trans. Antennas Propag.*, vol. 64, no. 6, pp. 2311–2318, Jun. 2016.

[16] M. Qing Qi, W. X. Tang, and T. J. Cui, "A broadband Bessel beam launcher using metamaterial lens," *Sci. Rep.*, vol. 5, no. 1, p. 11732, Jun. 2015.

[17] M. Ettorre and A. Grbic, "Generation of propagating Bessel beams using leaky-wave modes," *IEEE Trans. Antennas Propag.*, vol. 60, no. 8, pp. 3605–3613, Aug. 2012.

[18] W. Fuscaldo, G. Valerio, A. Galli, R. Sauleau, A. Grbic, and M. Ettorre, "Higher-order leaky-mode Bessel-beam launcher," *IEEE Trans. Antennas Propag.*, vol. 64, no. 3, pp. 904–913, Mar. 2016.

[19] E. Negri, W. Fuscaldo, M. Ettorre, P. Burghignoli, and A. Galli, "Analysis of resonant Bessel-beam launchers based on isotropic metasurfaces," in *16$^{\mathrm{th}}$ Eur. Conf. Antennas Propag. (EuCAP 2022)*, Madrid, Spain, 2022, pp. 1–4.

[20] P. Lu, A. Bréard, J. Huillery, X.-S. Yang, and D. Voyer, "Feeding coils design for TE-polarized Bessel antenna to generate rotationally symmetric magnetic field distribution," *IEEE Antennas Wireless Propag. Lett.*, vol. 17, no. 12, pp. 2424–2428, Dec. 2018.

[21] P. Lu, D. Voyer, A. Bréard, J. Huillery, B. Allard, X. Lin-Shi, and X.-S. Yang, "Design of TE-polarized Bessel antenna in microwave range using leaky-wave modes," *IEEE Trans. Antennas Propag.*, vol. 66, no. 1, pp. 32–41, Jan. 2017.

[22] D. Comite, W. Fuscaldo, S. K. Podilchak, P. D. Hílario-Re, V. Gómez-Guillamón Buendía, P. Burghignoli, P. Baccarelli, and A. Galli, "Radially periodic leaky-wave antenna for Bessel beam generation over a wide-frequency range," *IEEE Trans. Antennas Propag.*, vol. 66, no. 6, pp. 2828–2843, Jun. 2018.

[23] E. Negri, W. Fuscaldo, P. Burghignoli, and A. Galli, "A leaky-wave analysis of resonant Bessel-beam launchers: Design criteria, practical examples, and potential applications at microwave and millimeter-wave frequencies," *Micromachines*, vol. 13, no. 12, p. 2230, Dec. 2022.

[24] F. Benassi, W. Fuscaldo, E. Negri, G. Paolini, E. Augello, D. Masotti, P. Burghignoli, A. Galli, and A. Costanzo, "Comparison between hybrid- and TM-polarized Bessel-beam launchers for wireless power transfer in the radiative near-field at millimeter waves," in *51$^{\mathrm{st}}$ Eur. Microw. Conf. (EuMC 2021)*, London, UK, 2022, pp. 1–4.

[25] E. Negri, F. Benassi, W. Fuscaldo, D. Masotti, P. Burghignoli, A. Costanzo, and A. Galli, "Effective TE-polarized Bessel-beam excitation for wireless power transfer near-field links," in *52$^{\mathrm{nd}}$ Eur. Microw. Conf. (EuMC 2022)*, Milan, IT, 2022, pp. 1–4.

[26] Y. Xu, T. Peng, M. Sun, Y. Luo, J. Wang, W. Jiang, G. Liu, and Z. Wu, "Design and test of broadband rectangular waveguide TE_{10} to circular waveguide TE_{21} and TE_{01} mode converters," *IEEE Trans. Electron Devices*, vol. 66, no. 8, pp. 3573–3579, Aug. 2019.

[27] Q.-X. Chu, D.-Y. Mo, and Q.-S. Wu, "An isolated radial power divider via circular waveguide TE_{01}-mode transducer," *IEEE Trans. Microw. Theory Tech.*, vol. 63, no. 12, pp. 3988–3996, Dec. 2015.

[28] S. Paković, S. Zhou, D. González-Ovejero, S. C. Pavone, A. Grbic, and M. Ettorre, "Bessel–Gauss beam launchers for wireless power transfer," *IEEE Open J. Antennas Propag.*, vol. 2, pp. 654–663, 2021.

[29] E. Negri, F. Benassi, W. Fuscaldo, D. Masotti, P. Burghignoli, A. Costanzo, and A. Galli, "Design of TE-polarized resonant Bessel-beam launchers for wireless power transfer links in the radiative near-field region," *Int. J. Microw. Wirel. Technol.*, pp. 1–10, May 2024.

[30] V. R. Gowda, O. Yurduseven, G. Lipworth, T. Zupan, M. S. Reynolds, and D. R. Smith, "Wireless power transfer in the radiative near field," *IEEE Antennas Wirel. Propag. Lett.*, vol. 15, pp. 1865–1868, 2016.

[31] J. D. Heebl, E. M. Thomas, R. P. Penno, and A. Grbic, "Comprehensive analysis and measurement of frequency-tuned and impedance-tuned wireless non-radiative power-transfer systems," *IEEE Antennas Propag. Mag.*, vol. 56, no. 4, pp. 44–60, Aug. 2014.

[32] J. Garnica, R. A. Chinga, and J. Lin, "Wireless power transmission: From far field to near field," *Proc. IEEE*, vol. 101, no. 6, pp. 1321–1331, Apr. 2013.

[33] A. Galli, P. Baccarelli, and P. Burghignoli, "Leaky-wave antennas," Wiley, Ed. Hoboken, NJ: Wiley Online Library, 2016, pp. 1–20.

[34] V. Galdi and I. M. Pinto, "A simple algorithm for accurate location of leaky-wave poles for grounded inhomogeneous dielectric slabs," *Microw. Opt. Technol. Lett.*, vol. 24, no. 2, pp. 135–140, 2000.

[35] W. Fuscaldo, S. Tofani, D. C. Zografopoulos, P. Baccarelli, P. Burghignoli, R. Beccherelli, and A. Galli, "Systematic design of THz

leaky-wave antennas based on homogenized metasurfaces," *IEEE Trans. Antennas Propag.*, vol. 66, no. 3, pp. 1169–1178, Mar. 2018.
[36] W. Fuscaldo, A. Galli, and D. R. Jackson, "Optimization of 1-D unidirectional leaky-wave antennas based on partially reflecting surfaces," *IEEE Trans. Antennas Propag.*, vol. 70, no. 9, pp. 7853–7868, Sep. 2022.
[37] V. Rizzoli, A. Lipparini, A. Costanzo, F. Mastri, C. Cecchetti, A. Neri, and D. Masotti, "State-of-the-art harmonic-balance simulation of forced nonlinear microwave circuits by the piecewise technique," *IEEE Transactions Microw. Theory Techn.*, vol. 40, no. 1, pp. 12–28, Jan. 1992.
[38] W. Hallberg, M. Özen, D. Kuylenstierna, K. Buisman, and C. Fager, "A generalized 3-db Wilkinson power divider/combiner with complex terminations," *IEEE Trans. Microw. Theory Tech.*, vol. 66, no. 10, pp. 4497–4506, Oct. 2018.
[39] "CST products Dassault Systèmes, France, 2022." [Online]. Available: http://www.cst.com
[40] V. Rizzoli, D. Masotti, N. Arbizzani, and A. Costanzo, "CAD procedure for predicting the energy received by wireless scavenging systems in the near- and far-field regions," in *2010 IEEE MTT-S Int. Microw. Symp.*, 2010, pp. 1768–1771.
[41] G. Monti, D. Masotti, G. Paolini, L. Corchia, A. Costanzo, M. Dionigi, F. Mastri, M. Mongiardo, R. Sorrentino, and L. Tarricone, "EMC and EMI issues of WPT systems for wearable and implantable devices," *IEEE Electromagn. Compat. Mag.*, vol. 7, no. 1, pp. 67–77, 2018.

Walter Fuscaldo (Senior Member, IEEE) received the M.Sc. (cum laude) degree in Telecommunications Engineering from Sapienza University of Rome, Rome, in 2013. In 2017, he received the Ph.D. degree (cum laude and with the *Doctor Europaeus* label) in Information and Communication Technology (Applied Electromagnetics curriculum) from both the Department of Information Engineering, Electronics and Telecommunications (DIET) and the Institut d'Électronique et de Télécommunications de Rennes (IETR), Université de Rennes 1, Rennes, France, under a cotutelle agreement between the institutions. In 2014, 2017, 2018, he was a Visiting Researcher and in 2023 a Visiting Scientist with the NATO-STO Center for Maritime Research and Experimentation (CMRE), La Spezia, Italy. In 2016, he was a Visiting Researcher with the University of Houston, Houston, TX, USA. From July 2017 to June 2020, he was a Research Fellow at Sapienza University of Rome, and in July 2020, he joined the Institute for Microelectronics and Microsystems (IMM), Rome of the National Research Council (CNR) of Italy as a Researcher. His current research interests include propagation of leaky, surface, and plasmonic waves, leaky-wave antennas, generation of electromagnetic localized waves, graphene electromagnetics, metasurfaces, design of THz devices and THz spectroscopy. Dr. Fuscaldo was awarded several prizes, among which are the prestigious Young Engineer Prize for the Best Paper presented at the 46^{th} European Microwave Conference in 2016, London, UK and and the Best Paper in Electromagnetics and Antenna Theory at the 12^{th} European Conference on Antennas and Propagation in 2018. Since 2021 he has been included in the World's Top 2% Scientists' list by Stanford University.

Francesca Benassi (Member, IEEE) received the Ph.D. degree (cum laude) in Electronics, Telecommunications and Information Technologies Engineering from the University of Bologna, Bologna, Italy, in 2022. She is currently working as junior assistant professor at the Department of Electrical, Electronic and Information Engineering (DEI) "Guglielmo Marconi." Her main research interests involve the design of wearable rectennas for Wireless Power Transfer applications both at microwave and at millimeter waves. Dr. Benassi has been awarded with the MTT-S Graduate Fellowship Award and the EuMA Internship Award in 2021.

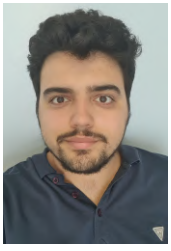

Edoardo Negri (Graduate Student Member, IEEE) was born in Orvieto, Italy, in 1997. He received the B.Sc. and M.Sc. degrees (cum laude) in electronic engineering, with honorable mention for the academic curriculum, from Sapienza University of Rome, Rome, Italy, in July 2019 and 2021, respectively, where he is currently pursuing the Ph.D. degree in Information and Communications Technologies (applied electromagnetics curriculum). From March to May 2023, Mr. Negri has been a visiting PhD student in the Institut d'Électronique et de Télécommunications de Rennes (IETR), Université de Rennes 1, Rennes, France, and, from September to November 2023 he has been a visiting PhD student in the Ferdinand-Braun-Institut, Leibniz-Institut für Höchstfrequenztechnik (FBH), Berlin, Germany. His main research interests are leaky waves, metasurfaces, focusing devices, and wireless near-field links at high frequencies (ranging from microwaves to terahertz). Mr. Negri received the "Antonio Ventura" Award as one of the best engineering students at the Sapienza University of Rome in 2022, the IEEE Antennas and Propagation Society (APS) Fellowship Award and the European Microwave Association (EuMA) Internship Award in 2023.

Giacomo Paolini (Member, IEEE) received the M.Sc. Degree in Biomedical Engineering and the Ph.D. Degree in Electronics, Telecommunications, and Information Technologies Engineering from the University of Bologna, Italy, in 2016 and 2021, respectively. He joined the Interdepartmental Center for Industrial Information and Communication Technologies Research (CIRI ICT) of the University of Bologna as a research fellow within the EU-supported HABITAT (Home Assistance Based on the Internet of Things for the AuTonomy of everybody) project in 2016. He is currently working as a junior assistant professor at the Department of Electrical, Electronic and Information Engineering "G. Marconi" (DEI) of the University of Bologna. His research interests include microwave radar systems for biomedical applications, indoor positioning exploiting RFID technologies, far-field wireless power transfer (WPT), and simultaneous wireless information and power transfer (SWIPT) systems.

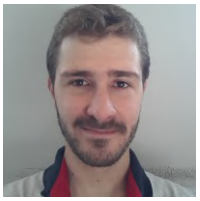

Francesco Maita earned his Master's degree, summa cum laude, in Electronics Engineering and a Ph.D. in "Engineering of Sensorial and Learning Systems" from the University of Rome Tor Vergata in 2008 and 2013, respectively. Since 2016, he has been a researcher at the Institute for Microelectronics and Microsystems of the CNR. In 2017, he became the lead for the Microoptoelectromechanical (MOEMS) systems workgroup. Additionally, since 2021, he has served as an expert referent for micro/nanolithography within the European network "Euronanolab." His research is centered on the design, fabrication, and characterization of advanced sensing systems, with a particular emphasis on flexible electronics and wireless sensor networks.

Paolo Burghignoli (Senior Member, IEEE) was born in Rome, Italy, in 1973. He received the Laurea degree (cum laude) in Electronic Engineering and the Ph.D. degree in Applied Electromagnetics from Sapienza University of Rome, Rome, Italy, in 1997 and 2001, respectively. In 1997, he joined the Department of Electronic Engineering, Sapienza University of Rome, where he is currently an Associate Professor with the Department of Information Engineering, Electronics and Telecommunications. He has authored about 250 articles in international journals, books, and conference proceedings. He is a co-author of the book *Electromagnetic Shielding: Theory and Applications* (Wiley-IEEE Press, 2023, 2nd ed.). His research interests include the analysis and design of planar antennas and arrays, leakage phenomena in uniform and periodic structures, numerical methods for integral equations and periodic structures, propagation and radiation in metamaterials, electromagnetic shielding, transient electromagnetics, and graphene electromagnetics. He is currently serving as an Associate Editor of the *IET Electronics Letters* and the *International Journal of Antennas and Propagation* (Hindawi).

Diego Masotti (Senior Member, IEEE) joined the University of Bologna in 1998 where he now serves as an Associate Professor of electromagnetic fields. From 2021 he has the role of coordinator of the Telecommunications Engineering Master Degree course. His research interests are in the areas of nonlinear microwave circuit simulation and design, with emphasis on nonlinear/electromagnetic co-design of integrated radiating subsystems/systems for wireless power transfer and energy harvesting applications. He authored more than 90 scientific publications on peer reviewed international journals and more than 190 scientific publications on proceedings of international conferences. Dr. Masotti is member of the IEEE MTT-25 Wireless Energy Transfer and Conversion Technical Committee and serves in the Editorial Board of Electronic Letters, of IEEE Access, of the IEEE Journal of RFID.

Alessandro Galli (Member, IEEE) received the Laurea degree in Electronics Engineering and the Ph.D. degree in Applied Electromagnetics from Sapienza University of Rome, Rome, Italy. Since 1990 he has been with the Department of Information Engineering, Electronics and Telecommunications at Rome Sapienza. He became an Assistant Professor and an Associate Professor in the sector of Electromagnetic Fields in 2000 and 2002, respectively. In 2013 he obtained the National Scientific Qualification, and later he definitively achieved the role of Full Professor in the same sector. His research interests concern various topics of guided-wave and radiation theory and applications, ranging from microwaves to terahertz. His activities also include topics of geoelectromagnetics, bioelectromagnetics, and plasma heating. He is the author of over 300 papers in international journals, books, and conference proceedings. Prof. Galli was elected Italian Representative in the Board of Directors of the European Microwave Association (EuMA) from 2010 to 2015. He was General Co-Chair of the 2014 European Microwave Week. He received various awards and recognitions for his research activity: in 2017 he was elected Best Teacher of the courses of the European School of Antennas (ESoA).

Alessandra Costanzo (Fellow, IEEE) is a full Professor in the Alma Mater Studiorum, Università di Bologna, ITALY. She is a Fellow of the IEEE, for contribution to “nonlinear electromagnetic co-design of RF and microwave circuits”. She has developed efficient design procedures based on the combination of electromagnetic and nonlinear numerical techniques, adopting both far-field and near-field solutions, thus creating the bridge between system-level and circuit-level analysis techniques of RF/microwave wireless links. She is currently the principal investigator of many research and industrial international projects at microwave and millimeter wave dedicated to Industrial IoT, and smart mobility. She is member of the Board of Directors of Rai Way S.p.A. since 2023. She has authored more than 300 scientific publications and owns four international patents. She is past associate editor of the IEEE Transaction on MTT, past Vice-President for publication of the IEEE CRFID.